A&A 630, A111 (2019)
https://doi.org/10.1051/0004-6361/201834940

Astronomy & Astrophysics

The WISSH quasars project

VI. Fraction and properties of BAL quasars in the hyper-luminosity regime

G. Bruni[1], E. Piconcelli[2], T. Misawa[3], L. Zappacosta[2], F. G. Saturni[2,4], G. Vietri[5,6], C. Vignali[7,8], A. Bongiorno[2], F. Duras[9,2], C. Feruglio[10,2], F. Tombesi[11,12,13,2], and F. Fiore[10]

[1] INAF – Istituto di Astrofisica e Planetologia Spaziali, Via Fosso del Cavaliere 100, 00133 Roma, Italy
e-mail: gabriele.bruni@inaf.it
[2] INAF – Osservatorio Astronomico di Roma, Via Frascati 33, 00040 Monte Porzio Catone, Roma, Italy
[3] School of General Education, Shinshu University 3-1-1 Asahi, Matsumoto 390-8621, Japan
[4] ASI – Space Science Data Center, Via del Politecnico snc, 00133 Roma, Italy
[5] Excellence Cluster Universe, Technische Universität München, Boltzmannstr. 2, 85748 Garching, Germany
[6] European Southern Observatory, Karl-Schwarzschild-Str. 2, 85748 Garching bei München, Germany
[7] DiFA – Dipartimento di Fisica e Astronomia, Università degli Studi di Bologna, Via Gobetti 93/2, 40129 Bologna, Italy
[8] INAF – Osservatorio di Astrofisica e Scienza dello Spazio di Bologna, Via Piero Gobetti 93/3, 40129 Bologna, Italy
[9] Dipartimento di Matematica e Fisica, Università degli Studi Roma Tre, Via della Vasca Navale 84, 00146 Roma, Italy
[10] INAF – Osservatorio Astronomico di Trieste, Via G.B. Tiepolo 11, 34143 Trieste, Italy
[11] Dipartimento di Fisica, Università degli Studi di Roma "Tor Vergata", Via della Ricerca Scientifica 1, 00133 Roma, Italy
[12] Department of Astronomy, University of Maryland, College Park, MD 20742, USA
[13] NASA/Goddard Space Flight Center, Code 662, Greenbelt, MD 20771, USA

Received 20 December 2018 / Accepted 20 August 2019

ABSTRACT

Context. The WISSH quasars project aims at studying the nuclear and host galaxy properties of the most luminous quasars ($L_{\rm bol} > 10^{47}$ erg s^{-1}, $1.8 < z < 4.6$), with special emphasis on the occurrence and physical parameters of winds at different scales.
Aims. Nuclear winds are manifested as UV-broad ($\geq$2000 km s^{-1}) absorption lines (BAL) in about 15% of quasars. We aim at studying the incidence and properties of such winds in the WISSH sample to investigate possible differences to active galactic nucleus regimes with lower luminosity.
Methods. We collected optical spectra from the Sloan Digital Sky Survey (SDSS) data release 12, and identified those showing absorption troughs in the region between the Si IV and C IV emission lines. We used three different indices for BAL absorption: the classic balnicity index (BI), the absorption index (AI), and the intermediate $\rm AI_{1000}$.
Results. We find a higher observed fraction of C IV BAL quasars in the WISSH sample (24%) than in previous catalogues (10–15%). These WISSH BAL quasars are also characterised by a higher average BI (~4000 km s^{-1}) and maximum velocity (~17 000 km s^{-1}). Moreover, for two objects we discovered BAL features bluewards of the Si IV peak, which can be associated with C IV absorption with a velocity of 0.15c. We also updated previous studies on the dependence of maximum outflow velocity upon bolometric luminosity, showing that BAL winds have intermediate properties compared to molecular or ionised winds and ultra-fast outflows. Finally, the radio properties of the WISSH BAL quasars as a whole are in line with those of samples at lower luminosities from previous studies.
Conclusions. Our results suggest that the higher $L_{\rm bol}$ of the WISSH quasars likely favours the acceleration of BAL outflows and that their most likely driving mechanism is radiation pressure. Furthermore, we estimate that the kinetic power associated with these winds in hyperluminous quasars for the highest column density and fastest winds is sufficient to provide efficient feedback onto the host galaxy.

Key words. galaxies: active – galaxies: nuclei – quasars: absorption lines – ISM: jets and outflows – quasars: general – quasars: supermassive black holes

1. Introduction

In the past two decades, the potential importance of the winds of quasi-stellar objects (QSOs) for the growth of super-massive black holes (SMBH, Silk & Rees 1998), for the enrichment of the intergalactic medium (Li et al. 2007), for galaxy formation (Haiman & Bryan 2006), for the evolution of the host galaxy (Di Matteo et al. 2005), and for the luminosity function of QSOs (Wyithe & Loeb 2003) has gained greater recognition. The power of the active galactic nucleus (AGN) is fundamental in the overall dynamics of the winds, therefore bolometric luminosity ($L_{\rm bol}$) and Eddington ratio are key quantities for understanding the mechanism of the feedback onto the host galaxy. Interaction of radiation, jets, and winds with the interstellar medium of the host is often invoked as responsible for star formation quenching and growth regulation, and it is commonly explained with two main scenarios: the radio mode, and the quasar mode (see Fabian 2012 for a review). In the former, the collimated radio jet is responsible for removing the ambient gas through fast shocks, while in the latter the main cause is identified as fast nuclear winds. Recently, both scenarios have proven to be valid: radio-mode feedback has been studied by Tadhunter et al. (2014), who presented evidence of a molecular outflow accelerated by the jet in a Seyfert galaxy, while Tombesi et al. (2015)

and Feruglio et al. (2015) pointed out that highly ionised massive SMBH winds with velocities of 0.1−0.2c are likely the drivers of kiloparsec-scale molecular winds with high outflow rates, that is, $\gtrsim$500 $M_\odot$ yr^{-1} (see Bischetti et al. 2019 for a more complete picture).

Nuclear winds from the accretion disc can be observed in the UV domain as broad absorption lines (BALs) blue-wards of prominent emission lines (e.g. C IV, Si IV) in 10−20% of the optically selected quasars. They trace wind velocities from a few thousand km s^{-1} up to ∼0.3c (e.g. Hewett & Foltz 2003; Hamann et al. 2018). Depending on the involved species, BALs are divided into high-ionisation (HiBALs) and low-ionisation (LoBALs) objects: while high-ionisation species (C IV, Si IV, N V) always produce the most prominent absorption features in these objects, about 15% also show troughs blue-wards of lower-ionisation species such as Mg II and Al III. Additionally, the LoBALs that also show Fe II and Fe III absorption features are called FeLoBALs. The number of known BAL QSOs has greatly increased in recent years based on the several data releases of the Sloan Digital Sky Survey (SDSS, York et al. 2000). More than 20 000 objects are listed in the recent releases of the SDSS quasar catalogue (Pâris et al. 2017, 2018). This allowed detailed studies of statistically complete samples, which helped to characterise the BAL phenomenology (see Sect. 3 for a complete discussion). Notwithstanding, a comprehensive scheme for the launching and geometry of BAL winds is still lacking, although some attempts of constructing reasonable scenarios exist (Murray & Chiang 1995; Proga 2000; Elvis 2000; Risaliti & Elvis 2010). Although theoretical models suggest that these winds should be launched by the accretion disc at a radius smaller than 1 pc (e.g. Proga 2000; Elvis 2000), observational results suggest to date that the distance at which the absorption occurs ranges from several tens to some thousand parsecs, and that luminous quasars have larger radii (see e.g. Arav et al. 2013; Hemler et al. 2019 and references therein). Recently, Arav et al. (2018) found evidence in a sample of about 20 high-luminosity QSOs that 50% of the BAL winds extend at least 100 pc from the nucleus. This highlights that these ionised outflows could indeed represent an important source of feedback to the host galaxy, although this is not in line with previous claims that BAL winds are located at scales of the AGN accretion disc.

Similarly, ultra-fast outflows (UFOs) are of nuclear origin as well, but are detected as absorption troughs in the X-ray domain; they trace higher-ionisation species at mildly relativistic velocities >0.1c (Tombesi et al. 2010, 2011). The origin of both BAL and UFO winds is thought to reside in the accretion disc and be driven by radiation pressure or magnetohydrodynamic processes (Laor & Brandt 2002; Tombesi et al. 2013; Kraemer et al. 2018). Radio emission from the jet was used by different authors as an indicator of the outflow orientation in samples of radio-loud BAL QSOs, but no clear indication of a preferred orientation was found (Montenegro-Montes et al. 2008; DiPompeo et al. 2011; Bruni et al. 2012). Very long-baseline (VLBI) observations showed a variety of morphologies (Bruni et al. 2013) that did not point towards a particular angle either, suggesting that BAL outflows and the consequent fraction of these objects among quasars might be due to the inner physical properties of the AGN, and not to a mere orientation effect. Indications of an anti-correlation with radio loudness have been found (Becker et al. 2000; Gregg et al. 2006; Shankar et al. 2008), while Hewett & Foltz (2003) suggested that optically bright BAL QSOs are half as likely as non-BAL QSOs to have $S_{1.4\,\mathrm{GHz}} > 1$ mJy.

The momentum and kinetic power of AGN winds at different scales are expected to increase with AGN bolometric luminosity (Menci et al. 2008; Zubovas & King 2012; Costa et al. 2014). There is mounting evidence that this prediction is correct based on observations at different wavelength of outflows involving different gas phases and distances from the SMBH (e.g. Cicone et al. 2014; Matzeu et al. 2017; Fiore et al. 2017). We have therefore undertaken a multi-band (from millimeter to X-rays) follow-up of a sample of 86 WISE/SDSS selected hyper-luminous (WISSH) QSOs in the redshift range $z \approx 2-4$, which is the so-called "cosmic noon" at the peak of star formation activity and QSO number density. The main goal is to provide a detailed investigation of nuclear and host galaxy properties and the census of AGN-driven winds in sources at the brightest end of the AGN luminosity function. WISSH QSOs exhibit very high bolometric luminosity ($L_{\rm bol} \gtrsim 10^{47}$ erg s^{-1}) powered by highly accreting ultra-massive (>10^9 $M_\odot$) SMBHs (see Bischetti et al. 2017; Duras et al. 2017; Martocchia et al. 2017; Vietri et al. 2018). These hyper-luminous AGN are thus expected to launch the most powerful outflows. By analysing rest-frame UV and optical spectra of WISSH QSOs, Bischetti et al. (2017) and Vietri et al. (2018) indeed reported on the discovery of ionised outflows both on kiloparsec and parsec scale, with extreme properties in terms of velocity and kinetic energy.

We here present a study of the fraction and properties of the BAL QSOs in the WISSH sample and discuss their dependence on the extreme bolometric luminosities of these objects. We adopt the latest cosmological parameters from the *Planck* mission (Planck Collaboration VI 2018), that is, assuming the base-ΛCDM cosmology: $H_0 = 67.4$ km s^{-1} Mpc^{-1}, $\Omega_{\rm m} = 0.315$, and $\Omega_\Lambda = 0.685$.

2. BAL identification from SDSS DR12 spectra

We performed a detailed search of BAL QSOs in the WISSH sample of 86 hyper-luminous QSOs, making use of SDSS optical spectra. At the mean redshift of the sample ($z \sim 3.2$), the SDSS observer's frame wavelength range (3500−9000 Å) corresponds to 830−2140 Å in the rest frame, allowing us to explore the whole region between the Lyα and Al III emission lines. Our aim was to test whether the BAL fraction, and thus the presence of nuclear winds, is different in the high-luminosity regime compared with previous estimates from the literature at lower luminosity ($L_{\rm bol} < 10^{47}$ erg s^{-1}). In the following, we describe the method and present details for the selection of BAL QSOs.

We collected optical spectra of all the 86 WISSH objects from the 12.0 data release of the SDSS (Alam et al. 2015). As a first selection step, we visually inspected them to find the footprint of absorption features blue-wards of the C IV emission peak. This led us to 42 candidate BAL QSOs (∼48% of the sample). Then, we fitted their spectra with the `continuum` tool in IRAF[1], using `spline3` as polynomial function, and flagging all the points that are part of the C IV absorption feature. With the obtained residuals, we characterised the broad absorption feature in velocity space, making use of three well-known indices from the literature: (1) the absorption index (AI), as defined in Hall et al. (2002),

$$\mathrm{AI} = \int_0^{25000} \left(1 - \frac{f(v)}{0.9}\right) \cdot C \mathrm{d}v, \quad (1)$$

where the parameter C is unity over contiguous troughs of at least 450 km s^{-1}; (2) the modified absorption index (AI_{1000}, Bruni et al. 2012), defined as in Hall et al. (2002), but where

[1] http://iraf.noao.edu/

the parameter C is unity over contiguous troughs of at least 1000 km s^{-1} (as in Trump et al. 2006); and (3) the balnicity index (BI), as defined by Weymann et al. (1991),

$$\mathrm{BI} = \int_{3000}^{25000} \left(1 - \frac{f(v)}{0.9}\right) \cdot C \mathrm{d}v, \quad (2)$$

where the parameter C is unity over contiguous troughs of at least 2000 km s^{-1}. To perform this calculation, the spectral region between the peaks of the C IV and Si IV emission lines was integrated up to 25 000 km s^{-1} from the former, starting from a minimum detachment of 0 km s^{-1} for AI and AI$_{1000}$, and 3000 km s^{-1} for BI. The three indices are increasingly conservative, from AI to BI; AI$_{1000}$ is the index that allows us to study a variety of absorption features, but still filters the most ambiguous features. Although they can be considered as velocity-weighted equivalent widths, they do not directly measure any outflow physical quantity, but instead can be used to quantify the strength and width of the absorption for BAL QSO identification purposes. Two of the objects presented here (0414+06 and 1210+17) are newly found BAL QSOs; they were not present in previous BAL catalogues (Trump et al. 2006; Gibson et al. 2009; Allen et al. 2011), nor were they flagged as BAL in the latest editions of the SDSS QSOs catalogue (Pâris et al. 2014, 2017 – the latter extracted from SDSS DR12 as for our sample). Both objects show problems in the spectrum that most probably misled the algorithm that was used for the compilation of previous catalogues: 0414+06 presents a spike in correspondence of the C IV peak, and 1210+17 has a spike at the right edge of the spectrum and a very faint Ly-α line that prevents easily identification of the Si IV and C IV emission lines. An incorrect redshift is given in SDSS for both objects, therefore we provide the corrected estimate in Table 1. In total, we found in WISSH 38 objects with an AI > 0 (44 ± 7%), 32 with AI$_{1000}$ > 0 (37 ± 6%), and 21 with BI > 0 (24 ± 5%), whose uncertainties are calculated with Poissonian statistics. Spectra for all the 38 BAL QSOs are given in Appendix A.

In addition to the classic selection based on C IV, we also searched for additional absorption from other species known to show BAL features, such as Si IV and Al III (Mg II was not covered by the spectra), with the aim to classify them into HiBAL or LoBAL objects. In order to quantify the absorption for these two species, we used a modified version of the previous indices, shifting the integration range blue-wards of the Si IV and Al III emission lines, respectively, and adopting the same maximum velocity of 25 000 km s^{-1}. Two objects show strong BAL features blue-wards of the Si IV emission line but only narrow absorption in the range between Si IV and C IV: we discuss these two particular cases in Sect. 3.3. The redshift of five objects prevented the Al III emission line region from lying in the SDSS wavelength range, therefore no classification into HiBAL or LoBAL was possible. The classification for all other sources is given in Table 1.

3. BAL fraction and strength in the extreme luminosity regime

3.1. BAL fraction in WISSH

The observed fraction of BAL QSOs ($\mathcal{F}_{\rm obs}$) in the total AGN population has been explored by several authors since the early 2000s. The main works that tried to compile BAL QSO catalogues and study their characteristics are the following: (1) Hewett & Foltz (2003), who presented a sample of 67 BAL QSOs from the large bright quasar survey (Hewett et al. 1995, pre-SDSS era), resulting in a $\mathcal{F}_{\rm obs} = 15 \pm 3\%$; (2) Reichard et al. (2003), who produced the first catalogue from an early data release of SDSS that included more than 200 objects, giving $\mathcal{F}_{\rm obs} = 14.0 \pm 1.0$; (3) Trump et al. (2006), who compiled objects from SDSS DR3, $\mathcal{F}_{\rm obs} \sim 10.4\%$; (4) Knigge et al. (2008), who worked based on SDSS DR3, $\mathcal{F}_{\rm obs} = 13.5$; (5) Gibson et al. (2009; G09 hereafter), who also worked based on SDSS DR5, $\mathcal{F}_{\rm obs} = 13.3 \pm 0.6\%$; and finally, (6) Allen et al. (2011), who used SDSS DR6, finding a dependence on redshift and an $\mathcal{F}_{\rm obs} = 8.0 \pm 0.1\%$. The common criterion adopted in these works to estimate $\mathcal{F}_{\rm obs}$ is the C IV BI. Considering the same definition of a BAL QSO, we find an observed fraction $\mathcal{F}^{W}_{\rm obs} = 24 \pm 5\%$ in WISSH with C IV BI > 0: this is almost twice the average fraction found in previous works, and 9% more than the largest fraction in these works. This points towards a intrinsic difference among WISSH BAL QSOs and previous samples that might be linked to the hyper-luminosity regime. Dai et al. (2008) investigated $\mathcal{F}_{\rm obs}$ in 2MASS-selected QSOs: they claimed a value of ∼40%, finding that BAL QSOs are redder than non-BAL QSOs, and suggesting that a negative selection bias prevents correctly estimating $\mathcal{F}_{\rm obs}$ in the optical band. Nevertheless, they found that a more restrictive classification based in BI leads to an $\mathcal{F}_{\rm obs} \sim 20$–$23\%$ (see their Fig. 6), which is more similar to the fractions found in optical band studies. This value is directly comparable and in agreement with the fraction we find for our sources. We also note that their 2MASS-selection (i.e. $K_s < 15.1$ mag) for $z > 1.7$ sources implies a selection of the most luminous QSOs with $M_{K_s} < -30$ mag in the optical rest-frame band[2]. As stated by Dai et al. (2008), only ∼5% of SDSS QSOs are detected in 2MASS because 2MASS is significantly shallower than the SDSS. This suggests that the luminosity mainly drives the increase in the BAL fraction.

We also estimated the fraction of LoBALs among BAL QSOs in WISSH. For 19 of the 21 objects with BI > 0, the spectrum covers the Al III region, which allows the LoBAL classification: for 5 of 19 objects, we obtained a Al III BI > 0, which means a LoBAL fraction of $\sim 26^{+18}_{-11}\%$ (following Poissonian statistics for small numbers, see Gehrels 1986). Generally, LoBALs can easily be missed in large surveys because of reddening and complex spectral features. The fraction found in WISSH is compatible within the errors with the fraction reported in the literature for SDSS objects (∼15%; e.g. Reichard et al. 2003; Sprayberry & Foltz 1992). Nevertheless, considering all C IV BI > 0 from G09 and applying the same criterion as above to identify LoBALs (i.e. C IV BI > 0 and Al III BI > 0), we find a much lower LoBAL fraction of 6.5 ± 0.4%: this could indicate that in the WISSH hyper-luminosity regime not only highly ionised gas outflows are more common, but also the lower-ionised component. This component might be launched from larger accretion disc radii and might more easily reach the relativistic velocities needed to produce BAL troughs.

In the remainder of the paper we consider the G09 catalogue as the comparison sample because it provides a more complete collection of wind parameters to be compared with our sample. In addition, we consider some quantities that were estimated in the Shen et al. (2011) QSOs catalogue based on SDSS DR7; Shen and collaborators adopted the BAL classification of G09. Considering all objects from G09 with a C IV BI > 0, we have a comparison sample of 4242 objects with redshift in the range $1.5 < z < 5.0$. In order to study the BAL wind

[2] The centroid of the K_s filter is centred in the rest-frame range 4000–8000 Å for their sources at $z = 1.7$–4.38.

Table 1. Forty BAL QSOs from the WISSH sample.

ID	SDSS ID	z	AI [km s^{-1}]	AI_{1000} [km s^{-1}]	BI [km s^{-1}]	v_{min} [km s^{-1}]	v_{max} [km s^{-1}]	Type
(1)	(2)	(3)	(4)	(5)	(6)	(7)	(8)	(9)
0045+14	SDSS004527.68+143816.1	1.992	7762	7718	7016	1300	16 000	**LoBAL**
0216−09	SDSS021646.94−092107.2	3.691	2335	1940	1170	8770	18 800	**HiBAL**
0414+06	SDSS041420.90+060914.2	2.614⋆	10 806	10 285	7415	1140	13 750	**HiBAL**
0747+27	SDSS074711.14+273903.3	4.110	209	12	0	2940	12 680	BAL
0928+53	SDSS092819.29+534024.1	4.390	9217	8327	8327	3430	19 050	**BAL**
0959+13	SDSS095937.11+131215.4	4.061	29	0	0	13 800	15 700	BAL
1013+56	SDSS101336.37+561536.3	3.633	127	0	0	3460	11 650	HiBAL
1025+24	SDSS102541.78+245424.2	2.382	3059	2866	2356	7260	13 750	**LoBAL**
1048+44	SDSS104846.63+440710.8	4.347	11 125	10 720	9044	2060	17 840	**BAL**
1051+31	SDSS105122.46+310749.3	4.243	203	14	0	9920	11 800	BAL
1103+10	SDSS110352.74+100403.1	3.590	357	38	0	1530	6160	HiBAL
1110+19	SDSS111017.13+193012.5	2.498	2680	2532	0	590	4900	HiBAL
1110+48	SDSS111038.63+483115.6	2.957	145	0	0	14 360	15 440	HiBAL
1122+16	SDSS112258.77+164540.3	3.024	8061	7861	7312	6610	17 670	**LoBAL**
1130+07	SDSS113017.37+073212.9	2.654	25	0	0	10 710	12 140	HiBAL
1157+27	SDSS115747.99+272459.6	2.217⋆	5641	4948	4021	2000	17 200	**HiBAL**
1204+33	SDSS120447.15+330938.7	3.596	5282	5117	3531	1620	10 590	**LoBAL**
1210+17	SDSS121027.62+174108.9	3.604⋆	5903	5595	5116	5840	14 750	**HiBAL**
1215−00	SDSS121549.81−003432.1	2.707	1679	1289	399	5800	20 640	**HiBAL**
1237+06	SDSS123714.60+064759.5	2.781	872	187	0	4200	19 810	HiBAL
1245+01	SDSS124551.44+010505.0	2.798	3707	3530	1939	1300	12 300	**HiBAL**
1250+20	SDSS125050.88+204658.7	3.570	890	824	0	350	3820	HiBAL
1305+05	SDSS130502.28+052151.1	4.071	246	42	0	19 500	22 550	HiBAL
1326−00	SDSS132654.96−000530.1	3.303⋆	2275	1960	0	0	3850	HiBAL
1328+58	SDSS132827.06+581836.8	3.133	322	131	0	3500	5400	HiBAL
1422+44	SDSS142243.02+441721.2	3.648⋆	310	0	0	15 410	22 780	HiBAL
1447+10	SDSS144709.24+103824.5	3.699	6179	4484	65	370	23 520	**HiBAL**
1451+14	SDSS145125.31+144136.0	3.102	4848	4340	3586	6000	13 400	**HiBAL**
1506+52	SDSS150654.55+522004.7	4.068	5147	4938	4396	12 970	23 130	**HiBAL**
1513+08	SDSS151352.52+085555.7	2.897	1293	820	0	200	4800	HiBAL
1544+41	SDSS154446.34+412035.7	3.548	4808	4663	4270	9580	23 500	**HiBAL**
1549+12	SDSS154938.72+124509.1	2.365⋆	4918	4425	1735	0	6470	**HiBAL**
1555+10	SDSS155514.85+100351.3	3.512	6992	6490	5576	7090	16 000	**LoBAL**
1633+36	SDSS163300.13+362904.8	3.576	377	241	90	18 700	24 800	**HiBAL**
1639+28	SDSS163909.10+282447.1	3.801	366	259	0	22 300	28 460	HiBAL
1650+25	SDSS165053.78+250755.4	3.338	3675	3516	2913	5000	13 100	**HiBAL**
2123−00	SDSS212329.46−005052.9	2.282⋆	107	0	0	13500	24 600	HiBAL
2238−08	SDSS223808.07−080842.1	3.122	4300	3889	2228	1500	19 000	**HiBAL**
0947+14	SDSS094734.19+142116.9	3.040	795	685	548	41 250	46 040	HiBAL
1538+08	SDSS153830.55+085517.0	3.567⋆	439	318	130	38 300	47 000	HiBAL

Notes. The first 38 objects are identified through absorption features between the Si IV and C IV emission lines, and the last 2 objects from features blue-wards of Si IV. Absorption index estimates are given in Cols. 4–6. In the last column, the BAL type is reported: objects with a C IV BI > 0 are set in bold face, while "BAL" means that the spectrum coverage does not allow a proper HiBAL/LoBAL classification. Redshifts with an asterisk are taken from Vietri et al. (2018).

dependence on L_{bol} and compare the G09 sample with the hyper-luminous objects from WISSH, we cross-correlated the C IV BI > 0 sample above with the Shen et al. (2011) QSOs catalogue (1 arcsec match in position) because this work provides the L_{bol} estimates we need for our analysis. This reduces the number of comparison BAL QSO objects to 3874.0 Fig. 1 (top panel) shows the L_{bol} distributions for the C IV BI > 0 objects from G09 and WISSH, and it highlights the extreme values of L_{bol} that are covered by the WISSH QSOs with respect to the previous samples.

3.2. BI distribution and BAL strength

As a further comparison with the G09 BAL QSOs population, we investigated the BI distributions for all objects with C IV BI > 0 from G09 and those from the WISSH sample: we found an excess of high BI values (see Fig. 1). A Kolmogorov-Smirnov (KS) test gives a $p < 0.05$ for the two distributions to be drawn from the same one.

G09 found a dependence of the BAL fraction from the spectral signal-to-noise ratio (S/N), with a higher S/N in the C IV

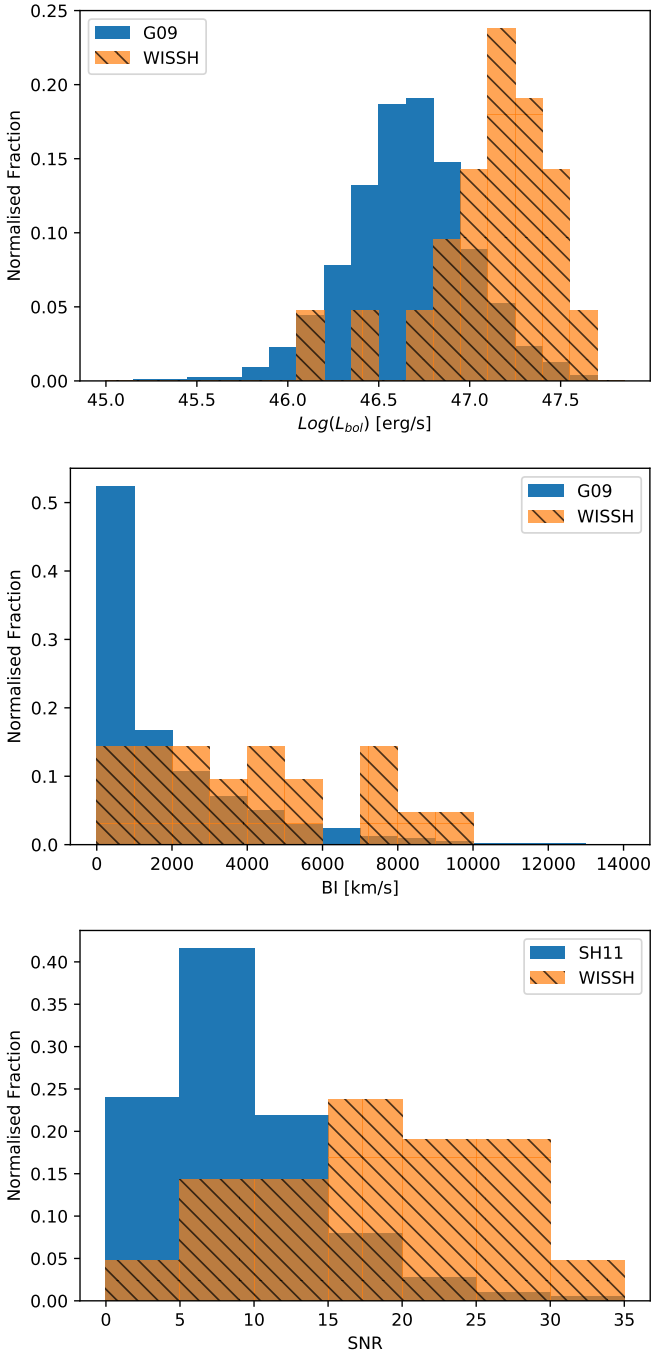

Fig. 1. *Top panel*: bolometric luminosity normalised distributions for WISSH and G09 objects with C IV BI > 0. *Middle panel*: C IV BI distribution for the WISSH sample and the BAL QSO catalogue from Gibson et al. (2009). *Bottom panel*: normalised distributions for the 1500−1600 Å S/N values extracted from SDSS DR7 for C IV BI > 0 BAL QSOs in WISSH and in the Shen et al. (2011) QSO catalogue (SH11).

region, which favours the identification of BAL troughs. This therefore enhances the fraction of BAL QSOs for a given sample. The WISSH sample is composed of high-luminosity objects (see Fig. 1), therefore a higher S/N is expected. To verify how much this effect could influence the fraction we measured in WISSH, we extracted the S/N of the 1500−1600 Å rest-frame non-absorbed region from the Shen et al. (2011) quasar catalogue for the objects with a BI > 0 in WISSH, and for all the objects that are flagged as BAL (as noted before, the Shen et al.

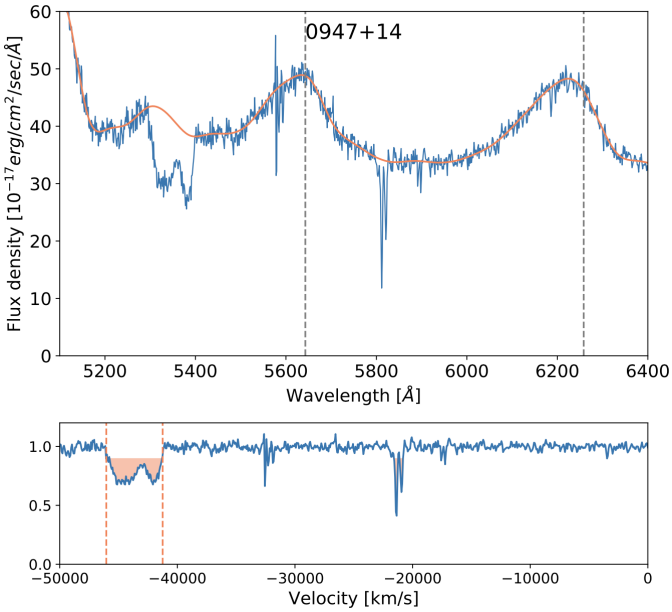

Fig. 2. Zoom on the C IV and Si IV regions for 0947+14 (SDSS DR12 spectrum), one of the two objects showing ultra-fast (>0.1c) BAL signatures associated with C IV absorption, blue-wards of the Si IV emission line. *Top panel*: spectrum (blue line) and fit performed in IRAF; dashed lines indicate the position of the Si IV and C IV peaks as calculated from the redshift. *Bottom panel*: residuals between the C IV peak and −50 000 km s^{-1}, with absorption below 90% of the continuum highlighted in orange; dashed lines indicate the minimum and maximum velocity estimated for the BAL outflow.

2011 BAL classification is taken from G09, and therefore it allows for a proper comparison). In Fig. 1 we compare the S/N distribution for WISSH BI > 0 objects with the distribution for all the BI > 0 objects from Shen et al. (2011). The mean S/N value increases in the two sets from a value of 9 per pixel for the Shen et al. (2011) objects to 18 for WISSH. Following G09, an increase in S/N from 9 to 18 implies a variation of about 2% more BAL QSOs. This contribution is clearly too low to justify the higher BAL QSO fraction we see in the WISSH sample with respect to the literature.

3.3. Detection of ultra-fast BAL outflows

In addition to the 38 C IV BAL QSOs presented in the previous section, we identified two more objects (0947+14 and 1538+08) with BAL signatures blue-wards of the Si IV emission line, but only very narrow absorption troughs between the C IV and Si IV lines (see Fig. 2). The optical depth ratio of the two species varies as a function of the ionisation parameter U, and for values typically found in BAL QSOs (Log(U) > −2), C IV dominates the Si IV depth by a factor of ∼2 (Dunn et al. 2012). The absence of strong absorption between the Si IV and C IV lines might therefore suggest that the BAL on the left side of Si IV is indeed due to C IV. This leads to a maximum velocity for the outflows in 0947+14 and 1538+08 of 0.15c and 0.16c, respectively. These ultra-fast BAL outflows (UBOs), which we conveniently define as BALs with a maximum velocity higher than 0.1c, which allows them to show C IV absorption blue-wards of the Si IV emission peak, are among the most extreme BALs detected to date. Although less common than slower BAL outflows, there is a growing census about UBOs in the literature (Rodríguez-Hidalgo et al. 2011;

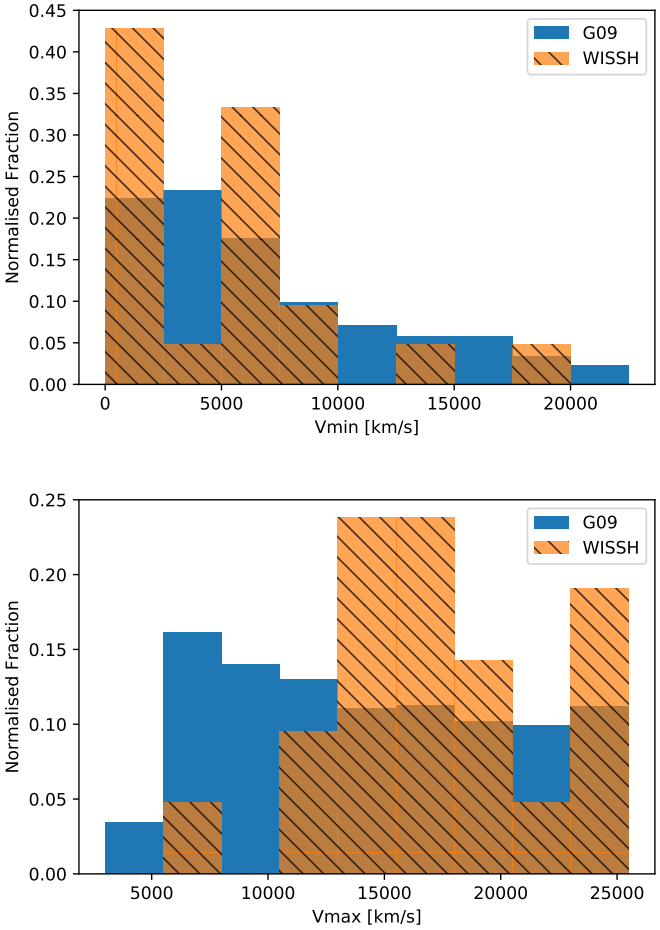

Fig. 3. Comparison between BI > 0 BAL QSOs $v_{\rm min}$ and $v_{\rm max}$ in the WISSH and G09 BAL QSO catalogue.

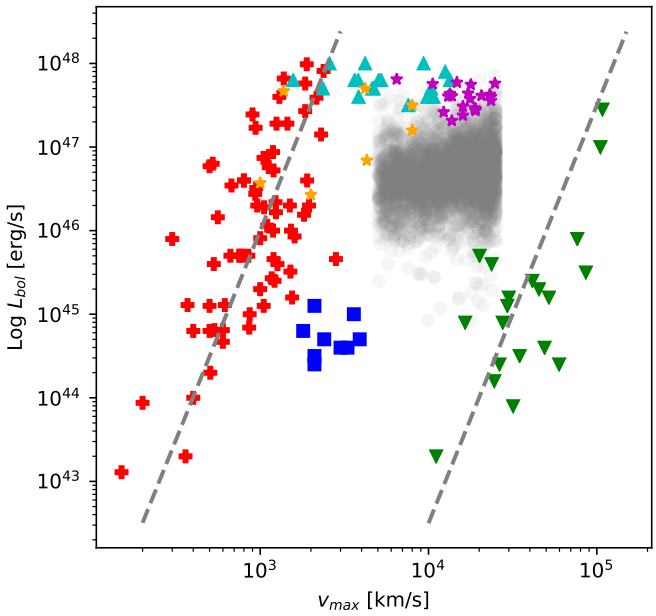

Fig. 4. Bolometric luminosities vs. maximum wind velocity for the objects in Fiore et al. (2017) (red crosses: molecular and ionised winds; blue squares: warm absorbers; green downwards triangles: UFOs; orange stars: BALs) for WISSH BI > 0 BAL QSOs (purple stars for the 21 C IV BALs), and for C IV winds from Vietri et al. (2018; cyan upwards triangles). The region occupied by the G09 objects with BI > 0 is shown in faded grey (the artificial $v_{\rm max}$ boundaries are a consequence of the BI selection).

Hamann et al. 2013; Rogerson et al. 2016), which in some cases present C IV absorption troughs blue-wards of the Lyα peak; this implies a velocity of ~0.3c (Hamann et al. 2018). A detailed analysis of multi-epoch UBOs properties in the WISSH sample will be presented in a forthcoming paper (Piconcelli et al., in prep.).

We explored the relative abundance of these relativistic BAL features in G09 by identifying all objects with Si IV BI > 0 and C IV BI = 0 in analogy to the two found in WISSH. In total, 2.9 ± 0.3% of objects in G09 show these characteristics (127 of the 4369 with Si IV or C IV BI > 0), while the fraction we obtain for WISSH is 9^{+11}_{-6}% (2 of 23 objects, i.e. the 21 C IV BI > 0 BAL QSOs plus the 2 UBOs themselves). This indicates a possible larger fraction of UBOs in high-luminosity QSOs such as WISSH. However, the very limited statistics hampers any firm conclusions on this trend, and additional investigations based on larger samples of QSOs with $L_{\rm bol} > 10^{47}$ erg s^{-1} are required.

3.4. Velocity distribution and potential for feedback of BAL QSOs

It is instructive to compare the distributions for the minimum and maximum velocities of the C IV BAL troughs ($v_{\rm min}$ and $v_{\rm max}$, respectively) for all the BI > 0 objects from both samples. We define as $v_{\rm min}$ and $v_{\rm max}$ the velocities estimated from the minimum and maximum wavelengths of the BAL troughs in the region between C IV and Si IV (values are given in Table 1). Normalised distributions for the two samples are plotted in Fig. 3.

The $v_{\rm max}$ distribution seems clearly different between the two samples; the WISSH QSOs exhibit a higher fraction at high velocities. A KS test gives a $p < 0.015$ for the $v_{\rm max}$ distribution from WISSH to be drawn from the same parent distribution as G09. This suggests that on average, hyperluminous QSOs host the more extreme manifestations of the BAL phenomenon. On the other hand, for the $v_{\rm min}$ distributions, the test suggests no significant difference between the two samples ($p > 0.15$).

It is tempting to associate $v_{\rm max}$ with the terminal velocity reached at larger distances (Ganguly et al. 2007). This may imply a more efficient acceleration mechanism for the most luminous QSOs, which pushes most of the winds up to $\gtrsim$15 000 km s^{-1}, that is, at the edge between the C IV and the Si IV emission lines used for the BI classification. As discussed above, the two UBOs show absorption even farther blue-ward of the Si IV line: this additionally indicates a larger velocity distribution for the WISSH QSOs with even higher $v_{\rm max}$ values. These results show that QSOs with extreme luminosities such as those in WISSH are able to accelerate BAL winds to higher velocities than are reached by AGN in lower luminosity regimes. G09 found a highly significant correlation between $L_{\lambda 2500}$ and $v_{\rm max}$, pointing towards a mainly radiative acceleration for the BAL winds, as suggested by previous authors (Murray & Chiang 1995; Laor & Brandt 2002).

In Fig. 4 we report $L_{\rm bol}$ as a function of $v_{\rm max}$ for a compilation of AGN-driven winds and outflows measured in different gas phases (molecular, ionised, warm absorbers, and UFOs). Data for molecular and ionised winds, warm absorbers, and UFOs have been collected by Fiore et al. (2017) with the specific aim of reporting properties of outflows with available estimates or limits on the physical distance of the high-velocity gas from the central engine. Figure 4 also includes the WISSH BI > 0 BAL QSOs together with the incomplete but representative list of

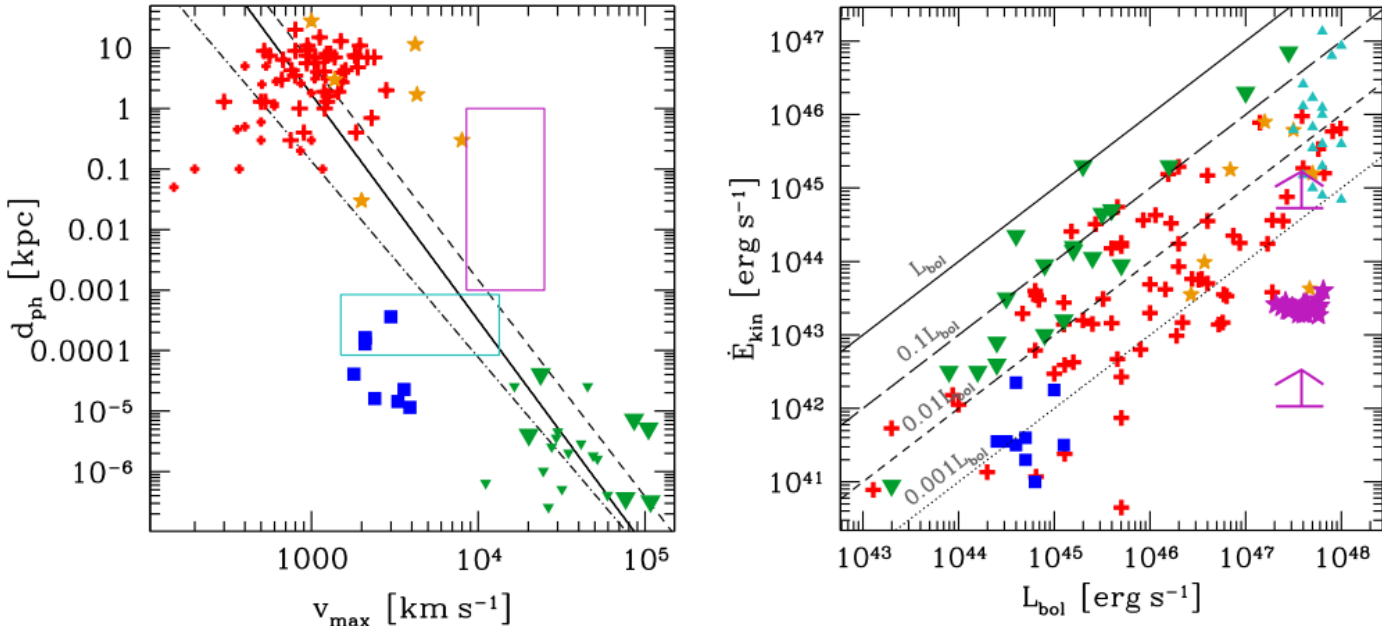

Fig. 5. *Left panel*: physical distance (d_{ph}) of the high-velocity outflow component as a function of v_{max} for the same sources as in Fig. 4 and belonging to the Fiore et al. (2017) sample. Large and small symbols for molecular and ionised kiloparsec-scale outflows (red crosses) and UFOs (green triangles) represent sources whose bolometric output is higher and lower than $\log(L_{bol}/erg\,s^{-1}) = 45.5$. Solid, dot-dashed, and dashed lines report the linear relations connecting the average points of kiloparsec-scale outflows and UFOs for all sources and sources fainter and brighter than $\log(L_{bol}/erg\,s^{-1}) = 45.5$, respectively. The position occupied by WISSH BALs and C IV broad emission line winds is reported with magenta and cyan rectangular regions, respectively (see text for details). *Right panel*: kinetic power as a function of bolometric luminosity for the sources reported in Fig. 4. The two lower limits represent our uncertainty on the BAL column density (see text for details).

BAL QSOs provided by Fiore et al. (2017). The reported L_{bol} for the WISSH BAL QSOs are estimated through spectral energy distribution (SED) fitting (Duras et al., in prep.), while for a good part of the sources reported in Fiore et al. (2017) L_{bol} is also estimated through bolometric correction factors. Fiore et al. (2017) found a log-linear relation between L_{bol} and v_{max} for both kiloparsc-scale molecular and ionised and nuclear sub-parsec relativistic winds with a similar slope of ∼5. The dependence is clearly visible in the plot, in which more luminous sources tend to exhibit faster and nuclear or kiloparsec-scale winds. In the plot we also report the 21 C IV WISSH BAL QSOs with BI > 0. For comparison, the position occupied by G09 BI > 0 BALs is also reported. Furthermore, we include broad C IV line nuclear winds that are detected as highly blue-shifted emission lines (Vietri et al. 2018). We mention that the log-linear relations found by Fiore et al. (2017) normalised to the average v_{max} of the WISSH BALs nicely cover the region occupied by the G09 BALs. This indicates a possible similar relation for this wind phase despite the large spread of values in the G09 BALs.

In the left panel of Fig. 5 we report the physical distance (d_{ph}) of the outflow measured for the high-velocity gas as a function of v_{max} for kiloparsec-scale outflows, WAs, BALs and UFOs, as reported in Fiore et al. (2017). We also include the locus occupied by BALs and C IV broad-emission-line nuclear winds that have been reported for the WISSH quasars. Because these winds do not have an actual distance estimate, we adopted the typical distances reported in literature studies. For WISSH BALs we adopted a range of 1 pc to 1 kpc (see e.g. Arav et al. 2018; Moravec et al. 2017; Leighly et al. 2018). For C IV broad-emission-line winds we adopted a range of ∼100−1000 light-days, which is typically found for luminous QSOs (e.g. $L_{bol} \approx 10^{47-48}$ erg s^{-1}) in reverberation mapping studies (e.g. Kaspi et al. 2007; Saturni et al. 2016). Overall, d_{ph} and v_{max} seem to be anti-correlated with nuclear winds; they exhibit faster winds than galaxy-scale outflows. We report in the figure a linear relation by joining the average points for kiloparsec-scale outflow and UFOs. There is an indication that this relation seems to be dependent on luminosity. We report with dot-dashed and dashed lines the relation for sources that are fainter and brighter than $\log(L_{bol}/erg\,s^{-1}) = 45.5$. Because (i) the data included in the fit lack uncertainties and (ii) the sample is incomplete, this relation must not be considered as universal, but just as an broad-brush indication of the inverse relation. We find relations with slopes −3.6 and −3.2 and a y-intercept 11.5 and 8.9 for bright and faint sources, respectively.

We used this relation between v_{max} and d_{ph} in order to estimate the maximum kinetic power $\dot{E}_{kin}$ associated with BAL outflows in WISSH QSOs. We inferred $\dot{E}_{kin}$ by dividing the kinetic energy $E_{kin} = 0.5 M v^2$ by a characteristic flow time given by d_{ph}/v_{max}. The kinetic energy was estimated as in Hamann et al. (2019). Their calculation assumed a spherical shell expanding at a certain velocity (v) with a given covering factor (Q) and smaller thickness than the radial distance (R). Under these assumptions, E_{kin} is expressed by the following formula:

$$E_{kin}^{max} \approx 1.7 \times 10^{54} \left(\frac{Q}{0.28}\right)\left(\frac{N_H}{5 \times 10^{22}\,cm^{-2}}\right)\left(\frac{R}{1\,pc}\right)^2 \times \left(\frac{v}{8000\,km\,s^{-1}}\right)^2 erg. \quad (3)$$

For our calculation we assumed $v = v_{max}$, $R = d_{ph}$ and $Q = 0.28$, which is the average value derived from the literature (Trump et al. 2006; Knigge et al. 2008; Gibson et al. 2009; Allen et al. 2011). Because we do not have information on the column densities, and because estimating them is beyond the aim of this work, we adopted a value of $N_H = 2.2 \times 10^{21}$ cm^{-2}. This is the logarithmic mean value between of $N_H = 10^{20}$ cm^{-2} and $N_H = 5 \times 10^{22}$ cm^{-2}, which are minimum column densities derived from doubly and triply ionised species

Arav et al. (2018) and P V troughs Hamann et al. (2019), respectively. In the right panel of Fig. 5 we report the $\dot{E}_{\rm kin}$ estimated for the WISSH BALs as a function of $L_{\rm bol}$ compared to the same values reported for other winds or outflows by Fiore et al. (2017) and Vietri et al. (2018). We report as lower limits the values of $\dot{E}_{\rm kin}$ estimated at the minimum $N_{\rm H}$ reported for low column density Arav et al. (2018) and high column density (i.e. from P V troughs, Arav et al. 2018) winds. The densest winds can reach values of the kinetic power that are about $\gtrsim$0.1% of the bolometric luminosity. Even higher values are expected if the luminosity dependence of the $d_{\rm ph} - v_{\rm max}$ relation holds at highest luminosities. We assumed that most of the outflowing mass is carried at $v_{\rm max}$. When we instead adopt $v_{\rm min}$ as representative phase for carrying the majority of the kinetic power of the wind, then by adopting the lowest value of $d_{\rm ph}$ = 1 pc, we obtain a lower limit on $\dot{E}_{\rm kin}$ that is one order of magnitude lower. Bearing in mind the crude assumptions in this estimate, this is an indication that some of these winds are in principle able to transport a kinetic power sufficient for generating a significant feedback contribution on the host (Di Matteo et al. 2005; Hopkins & Elvis 2010).

3.5. Multiple AGN winds in WISSH quasars

Bischetti et al. (2017) and Vietri et al. (2018) revealed kiloparsec- and BLR-scale winds in WISSH objects by detecting a broad- and blue-shifted [OIII], or C IV emission lines in the rest-frame, optical, and UV spectra of a randomly selected sub-sample of 18 WISSH QSOs. Seven of these objects (1157+27, 1326−00, 1421+46, 1422+44, 1538+08, 1549+12, and 2123−00) exhibit absorption features in their SDSS spectra (see Table 1). Specifically, they all show an $\rm AI_{1000} > 0\,km\,s^{-1}$), and for four sources we derive a positive BI. Vietri et al. (2018) reported two sub-populations of WISSH QSOs based on their emission line properties. The first (consisting of six sources, dubbed [OIII] is characterised by a broad [OIII], emission line, a rest-frame equivalent width (REW) of the C IV emission $\rm REW_{CIV} \approx 20-40$ Å and a profile of the C IV emission line blue-shifted of $<$2000 km s^{-1}. The second population (dubbed Weak [OIII] sources, which represents two-thirds of the LBT/LUCI WISSH sample) exhibits weak or entirely absent [OIII] emission, and a highly blue-shifted (2000−8000 km s^{-1}) C IV emission line with REW $<$ 20 Å.

Vietri et al. (2018) interpreted the dichotomy observed in WISSH QSOs in terms of a combination of huge ionising flux (leading to overionisation of the NLR gas and thereby to a decrease in the [OIII] emission, e.g. Shen & Ho 2014) and inclination. In particular, for Weak [OIII] QSOs the accretion disc is seen face-on, while [OIII] QSOs are expected to be viewed at larger inclination angles, that is, $\theta \sim 25-70°$. Interestingly, intermediate inclinations (∼25−40°) for BAL QSOs have also been suggested by Elvis (2000).

Of the seven QSOs with AI > 0 km s^{-1}, three belong to the [OIII] subclass, and four are Weak [OIII] objects. Two out of three [OIII] QSOs are classified as BAL according to BI, and the remaining one (1326−00) has $\rm AI_{1000} \lesssim 2000\,km\,s^{-1}$. This is quite interesting and suggests that the simultaneous presence of BAL and kiloparsec-scale outflows may be common at the highest AGN luminosities. In contrast, only one Weak [OIII] QSO (1157+27) shows a BI > 0 km s^{-1}, and all the remaining ones only have modest ($\lesssim$300 km s^{-1}) AI. Future follow-up studies of the [OIII] emission in a larger sample of luminous BAL QSOs will be crucial to support this orientation scenario for the simultaneous detection of NLR and BAL outflows.

4. Radio properties of WISSH BAL QSOs

We cross-correlated the BAL QSOs list from WISSH with the FIRST catalogue (Becker et al. 1995), using a 5″ matching radius centred on the optical coordinates in order to determine the fraction of WISSH BAL QSOs with a radio counterpart. Eight of 38 (∼21%) have a counterpart in FIRST: 0747+27, 1025+24, 1130+07, 1204+33, 1237+06, 1422+44, 1513+08, and 1549+12. As a whole, 20 of 86 objects (∼23%) in WISSH have a radio counterpart.

Shankar et al. (2008) studied the dependence of the BAL QSOs fraction among the radio population as a function of specific luminosity at 1.4 GHz ($L_{\rm 1.4\,GHz}$, from FIRST). They found that it can drop from ∼20% to ∼8% from an $L_{\rm 1.4\,GHz} \sim 10^{32}$ to $\sim 10^{36}$ erg s^{-1} Hz^{-1} for BI-selected BAL QSOs, and from ∼45% to ∼20% for the AI-selected ones. No entirely satisfactory physical model was found for this behaviour, both the evolutionary and geometrical model do not reflect the complex phenomenology of these objects. The $L_{\rm 1.4\,GHz}$ range for the WISSH sample is $8 \times 10^{31}-2 \times 10^{35}$ erg s^{-1} Hz^{-1} (see Fig. 6), similar to the range explored by those authors. This was calculated from the FIRST flux density as in Eq. (1) of Shankar et al. (2008), but assuming a spectral index $\alpha = 0$ because both inverted and steep spectral indices have been found in samples of radio-loud BAL QSOs (Montenegro-Montes et al. 2008; DiPompeo et al. 2011; Bruni et al. 2012), although, as discussed in Shankar et al. (2008), the estimate only weakly depends on α. Despite the poor statistics (only 8 of the 20 WISSH objects with a radio counterpart are BAL QSOs), the fraction we find at luminosities $L_{\rm 1.4\,GHz} < 10^{33}$ erg s^{-1} Hz^{-1} is ∼47% when objects with AI > 0 are considered, and it is ∼20% when objects with BI > 0 are considered, in agreement with the trend found by these authors.

From a morphological point of view, images from FIRST show a compact morphology for all sources, corresponding to an upper limit for linear sizes of ∼40 kpc at the mean redshift of the BAL QSOs sub-sample in WISSH ($z = 3.2$). This is in agreement with linear sizes from previous studies at arcsec angular resolution (Bruni et al. 2012), resulting in a compact radio morphology, <40 kpc, for more than 90% of the objects at a similar redshift range.

The radio properties presented here do not suggest a behaviour different from previous samples, despite the extreme luminosity regime in WISSH. The coupling between the BAL-producing winds and the jet seems to have trends similar to those presented in previous works from the literature, meaning that the higher probability for WISSH objects to launch winds does not imply different jet formation rates or strength.

5. Conclusions

We have analysed the properties of the BAL QSOs fraction in the WISSH sample, which is composed of hyper-luminous type 1 AGN, and compared them to the BAL QSOs from the literature. Our results can be summarised as follows:

– Adopting the standard BAL indices, we found 38 objects in WISSH with an AI > 0 (44 ± 7%), 32 with $\rm AI_{1000} > 0$ (37 ± 6%), and 21 with BI > 0 (24 ± 5%).
– The fraction of objects with a C IV BI > 0 (24%) is almost twice higher than what was found in G09. Moreover, the BI distributions for the two samples are distinct, with typically higher values for the WISSH sample. The LoBAL fraction of the BAL QSOs in WISSH is ∼26%, which is also larger than what was found at similar luminosities in previous works. The higher $L_{\rm bol}$ of the WISSH objects likely

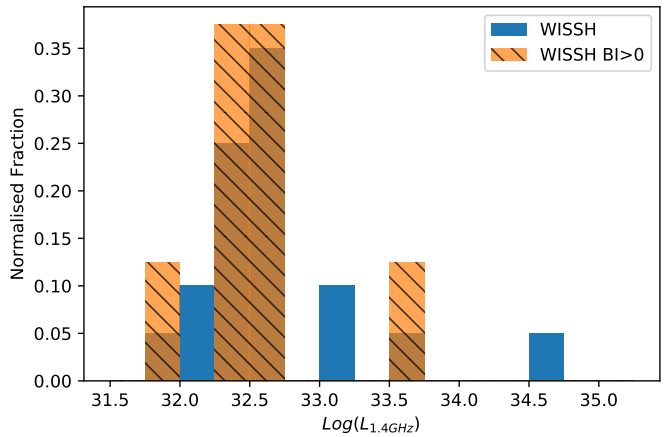

Fig. 6. Normalised distributions of $L_{1.4\,\mathrm{GHz}}$ for all WISSH objects with a FIRST radio counterpart (blue) and for BAL QSOs in WISSH with a FIRST radio counterpart (orange).

favours the acceleration of BAL outflows (in both the high- and low-ionisation gas components), indicating that they are likely radiatively driven.

– The maximum velocities of the C IV BAL outflows in WISSH have a different distribution from those in G09, with WISSH QSOs exhibiting higher values. This lends further support to the theoretical predictions that have suggested that hyper-luminous QSOs are able to launch the most extreme winds through radiative pressure (Giustini & Proga 2019).
– We find two QSOs with BAL features with velocities of $\sim 0.15c$ by assuming that absorption blue-wards of the Si IV emission line is associated with C IV. Although the statistics is very limited (i.e. 2 of the 21 objects show a BI > 0), this seems to lend further support to a scenario where hyper-luminous QSOs are able to accelerate the most powerful outflows (e.g. Laor & Brandt 2002; Fiore et al. 2017)
– We estimated the possible range of kinetic power associated with BAL outflows in WISSH, which can reach values above 0.1% of L_{bol}. This indicates that especially for the highest column density and fastest winds, BAL outflows in hyperluminous QSOs might be able to provide an efficient feedback onto the interstellar medium of the host galaxy.
– About 20% of the BI-selected BAL QSOs from WISSH shows a radio counterpart in FIRST (1.4 GHz), this fraction is compatible with the one found in G09 (23%). It also confirms that the WISSH sample shows the same anti-correlation between $L_{1.4\,\mathrm{GHz}}$ and the BAL QSOs abundance found by Shankar et al. (2008), and it does not indicate any particular dependence of the BAL QSO radio properties on the L_{bol}.

Future works based on much larger samples of hyper-luminous QSOs are needed to shed more light on the crucial role of L_{bol} in increasing the fraction and the power of BAL outflows in the QSO population.

Acknowledgements. We thank the anonymous referee for the constructive comments and suggestions. GB acknowledges financial support under the INTEGRAL ASI-INAF agreement 2013-025-R.1. EP acknowledges financial support from the Italian Space Agency (ASI) under the contracts ASI-INAF I/037/12/0 and ASI-INAF n.2017-14-H.0. LZ acknowledges financial support under ASI/INAF contract I/037/12/0. FT acknowledges support by the Programma per Giovani Ricercatori – anno 2014 Rita Levi Montalcini. This research project was supported by the DFG Cluster of Excellence "Origin and Structure of the Universe" (www.universe-cluster.de). Funding for the Sloan Digital Sky Survey IV has been provided by the Alfred P. Sloan Foundation, the US Department of Energy Office of Science, and the Participating Institutions. SDSS-IV acknowledges support and resources from the Center for High-Performance Computing at the University of Utah. The SDSS web site is www.sdss.org. SDSS-IV is managed by the Astrophysical Research Consortium for the Participating Institutions of the SDSS Collaboration including the Brazilian Participation Group, the Carnegie Institution for Science, Carnegie Mellon University, the Chilean Participation Group, the French Participation Group, Harvard-Smithsonian Center for Astrophysics, Instituto de Astrofísica de Canarias, The Johns Hopkins University, Kavli Institute for the Physics and Mathematics of the Universe (IPMU)/University of Tokyo, the Korean Participation Group, Lawrence Berkeley National Laboratory, Leibniz Institut für Astrophysik Potsdam (AIP), Max-Planck-Institut für Astronomie (MPIA Heidelberg), Max-Planck-Institut für Astrophysik (MPA Garching), Max-Planck-Institut für Extraterrestrische Physik (MPE), National Astronomical Observatories of China, New Mexico State University, New York University, University of Notre Dame, Observatário Nacional/MCTI, The Ohio State University, Pennsylvania State University, Shanghai Astronomical Observatory, United Kingdom Participation Group, Universidad Nacional Autónoma de México, University of Arizona, University of Colorado Boulder, University of Oxford, University of Portsmouth, University of Utah, University of Virginia, University of Washington, University of Wisconsin, Vanderbilt University, and Yale University.

References

Alam, S., Albareti, F. D., Allende Prieto, C., et al. 2015, ApJS, 219, 12
Allen, J. T., Hewett, P. C., Maddox, N., Richards, G. T., & Belokurov, V. 2011, MNRAS, 410, 860
Arav, N., Borguet, B., Chamberlain, C., Edmonds, D., & Danforth, C. 2013, MNRAS, 436, 3286
Arav, N., Liu, G., Xu, X., et al. 2018, ApJ, 857, 60
Becker, R. H., White, R. L., & Helfand, D. J. 1995, ApJ, 450, 559
Becker, R. H., White, R. L., Gregg, M. D., et al. 2000, ApJ, 538, 72
Bischetti, M., Piconcelli, E., Vietri, G., et al. 2017, A&A, 598, A122
Bischetti, M., Piconcelli, E., Feruglio, C., et al. 2019, A&A, 628, A118
Bruni, G., Mack, K. H., Salerno, E., et al. 2012, A&A, 542, A13
Bruni, G., Dallacasa, D., Mack, K. H., et al. 2013, A&A, 554, A94
Cicone, C., Maiolino, R., Sturm, E., et al. 2014, A&A, 562, A21
Costa, T., Sijacki, D., & Haehnelt, M. G. 2014, MNRAS, 444, 2355
Dai, X., Shankar, F., & Sivakoff, G. R. 2008, ApJ, 672, 108
Di Matteo, T., Springel, V., & Hernquist, L. 2005, Nature, 433, 604
DiPompeo, M. A., Brotherton, M. S., De Breuck, C., & Laurent-Muehleisen, S. 2011, ApJ, 743, 71
Dunn, J. P., Arav, N., Aoki, K., et al. 2012, ApJ, 750, 143
Duras, F., Bongiorno, A., Piconcelli, E., et al. 2017, A&A, 604, A67
Elvis, M. 2000, ApJ, 545, 63
Fabian, A. C. 2012, Ann. Rev. Astron. Astrophys., 50, 455
Feruglio, C., Fiore, F., Carniani, S., et al. 2015, A&A, 583, A99
Fiore, F., Feruglio, C., Shankar, F., et al. 2017, A&A, 601, A143
Ganguly, R., Brotherton, M. S., Cales, S., et al. 2007, ApJ, 665, 990
Gehrels, N. 1986, ApJ, 303, 336
Gibson, R. R., Jiang, L., Brandt, W. N., et al. 2009, ApJ, 692, 758
Giustini, M., & Proga, D. 2019, A&A, 630, A94
Gregg, M. D., Becker, R. H., & de Vries, W. 2006, ApJ, 641, 210
Haiman, Z., & Bryan, G. L. 2006, ApJ, 650, 7
Hall, P. B., Anderson, S. F., Strauss, M. A., et al. 2002, ApJS, 141, 267
Hamann, F., Chartas, G., McGraw, S., et al. 2013, MNRAS, 435, 133
Hamann, F., Chartas, G., Reeves, J., & Nardini, E. 2018, MNRAS, 476, 943
Hamann, F., Herbst, H., Paris, I., & Capellupo, D. 2019, MNRAS, 483, 1808
Hemler, Z. S., Grier, C. J., Brandt, W. N., et al. 2019, ApJ, 872, 21
Hewett, P. C., & Foltz, C. B. 2003, AJ, 125, 1784
Hewett, P. C., Foltz, C. B., & Chaffee, F. H. 1995, AJ, 109, 1498
Hopkins, P. F., & Elvis, M. 2010, MNRAS, 401, 7
Kaspi, S., Brandt, W. N., Maoz, D., et al. 2007, ApJ, 659, 997
Knigge, C., Scaringi, S., Goad, M. R., & Cottis, C. E. 2008, MNRAS, 386, 1426
Kraemer, S. B., Tombesi, F., & Bottorff, M. C. 2018, ApJ, 852, 35
Laor, A., & Brandt, W. N. 2002, ApJ, 569, 641
Leighly, K. M., Terndrup, D. M., Gallagher, S. C., Richards, G. T., & Dietrich, M. 2018, ApJ, 866, 7
Li, Y., Hernquist, L., Robertson, B., et al. 2007, ApJ, 665, 187
Martocchia, S., Bastian, N., Usher, C., et al. 2017, MNRAS, 468, 3150
Matzeu, G. A., Reeves, J. N., Braito, V., et al. 2017, MNRAS, 472, L15
Menci, N., Fiore, F., Puccetti, S., & Cavaliere, A. 2008, ApJ, 686, 219
Montenegro-Montes, F. M., Mack, K. H., Vigotti, M., et al. 2008, MNRAS, 388, 1853
Moravec, E. A., Hamann, F., Capellupo, D. M., et al. 2017, MNRAS, 468, 4539
Murray, N., & Chiang, J. 1995, ApJ, 454, L105
Pâris, I., Petitjean, P., Aubourg, É., et al. 2014, A&A, 563, A54

Pâris, I., Petitjean, P., Ross, N. P., et al. 2017, A&A, 597, A79
Pâris, I., Petitjean, P., Aubourg, É., et al. 2018, A&A, 613, A51
Planck Collaboration VI. 2018, A&A, submitted [arXiv:1807.06209]
Proga, D. 2000, ApJ, 538, 684
Reichard, T. A., Richards, G. T., Schneider, D. P., et al. 2003, AJ, 125, 1711
Risaliti, G., & Elvis, M. 2010, A&A, 516, A89
Rodríguez-Hidalgo, P., Hamann, F., & Hall, P. 2011, MNRAS, 411, 247
Rogerson, J. A., Hall, P. B., Rodríguez Hidalgo, P., et al. 2016, MNRAS, 457, 405
Saturni, F. G., Trevese, D., Vagnetti, F., Perna, M., & Dadina, M. 2016, A&A, 587, A43
Shankar, F., Dai, X., & Sivakoff, G. R. 2008, ApJ, 687, 859
Shen, Y., & Ho, L. C. 2014, Nature, 513, 210
Shen, Y., Richards, G. T., Strauss, M. A., et al. 2011, ApJS, 194, 45
Silk, J., & Rees, M. J. 1998, A&A, 331, L1
Sprayberry, D., & Foltz, C. B. 1992, ApJ, 390, 39
Tadhunter, C., Morganti, R., Rose, M., Oonk, J. B. R., & Oosterloo, T. 2014, Nature, 511, 440
Tombesi, F., Cappi, M., Reeves, J. N., et al. 2010, A&A, 521, A57
Tombesi, F., Cappi, M., Reeves, J. N., et al. 2011, ApJ, 742, 44
Tombesi, F., Cappi, M., Reeves, J. N., et al. 2013, MNRAS, 430, 1102
Tombesi, F., Meléndez, M., Veilleux, S., et al. 2015, Nature, 519, 436
Trump, J. R., Hall, P. B., Reichard, T. A., et al. 2006, ApJS, 165, 1
Vietri, G., Piconcelli, E., Bischetti, M., et al. 2018, A&A, 617, A81
Weymann, R. J., Morris, S. L., Foltz, C. B., & Hewett, P. C. 1991, ApJ, 373, 23
Wyithe, J. S. B., & Loeb, A. 2003, ApJ, 595, 614
York, D. G., Adelman, J., Anderson, Jr., J. E., et al. 2000, AJ, 120, 1579
Zubovas, K., & King, A. 2012, ApJ, 745, L34

Appendix A: BAL QSOs spectra

We report here the SDSS DR12 spectra of the 38 BAL QSOs presented in this work. For each object, we show the spectrum, the combined continuum and emission line fit performed in IRAF, the Si IV and C IV peak positions as calculated from redshift (dashed grey lines), and the residuals used to calculate the BAL index integrals (from 0 to 25 000 km s^{-1}), where the absorption below 90% of the continuum is highlighted in orange. We also mark the $v_{\rm min}$ and $v_{\rm max}$ estimates for each object with dashed orange lines.

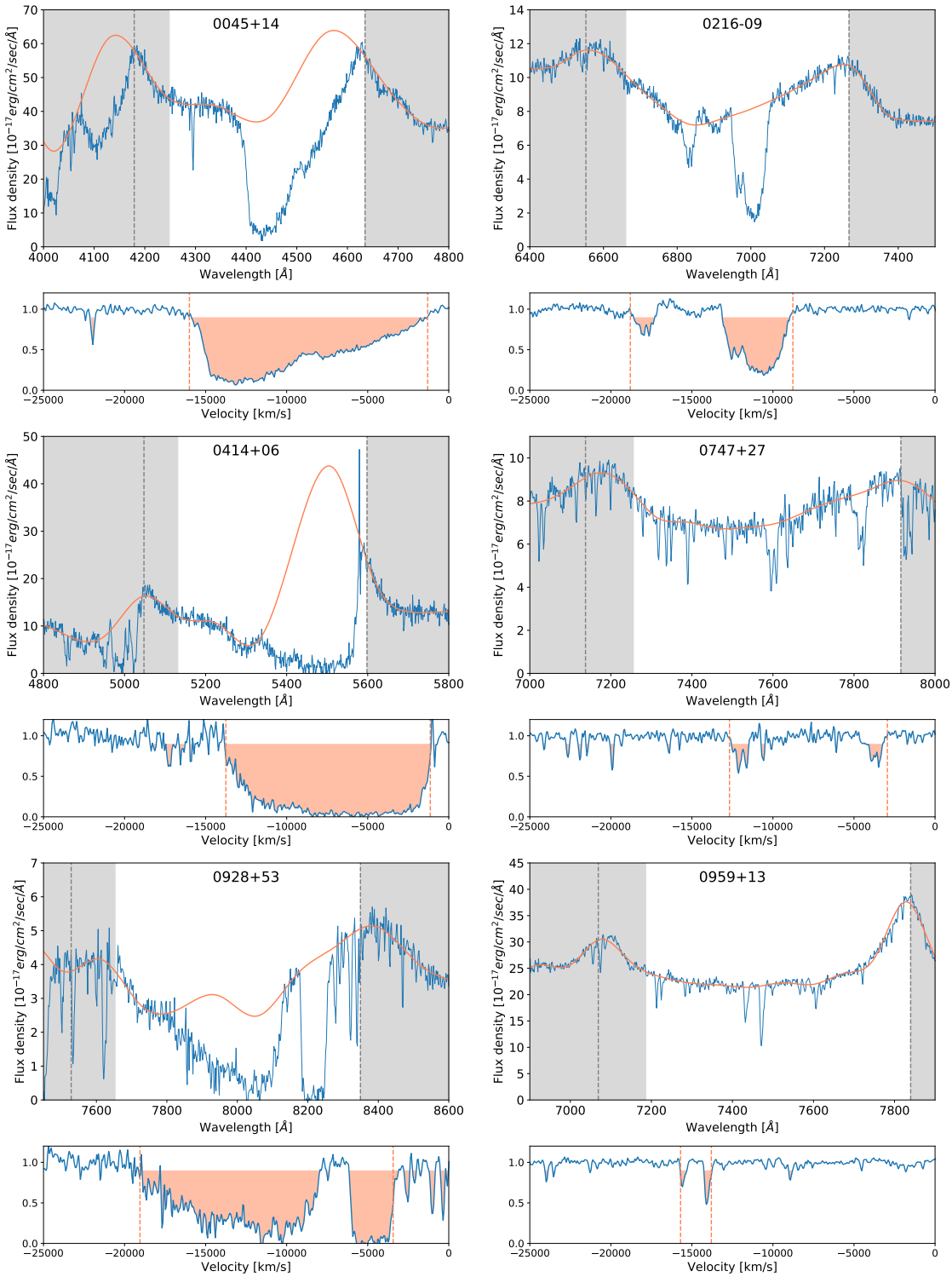

Fig. A.1. SDSS DR12 spectra of the 38 BAL QSOs presented here. *Top panel*: spectrum (blue line) and fit performed in IRAF (orange line); dashed lines indicate the position of the Si IV and C IV peaks as calculated from redshift, and the white area denotes the wavelength interval between 0 and −25 000 km s^{-1}. *Bottom panel*: residuals between the C IV peak and −25 000 km s^{-1}; absorption below 90% of the continuum is highlighted in orange; the dashed lines indicate the minimum and maximum velocity estimated for the BAL outflow.

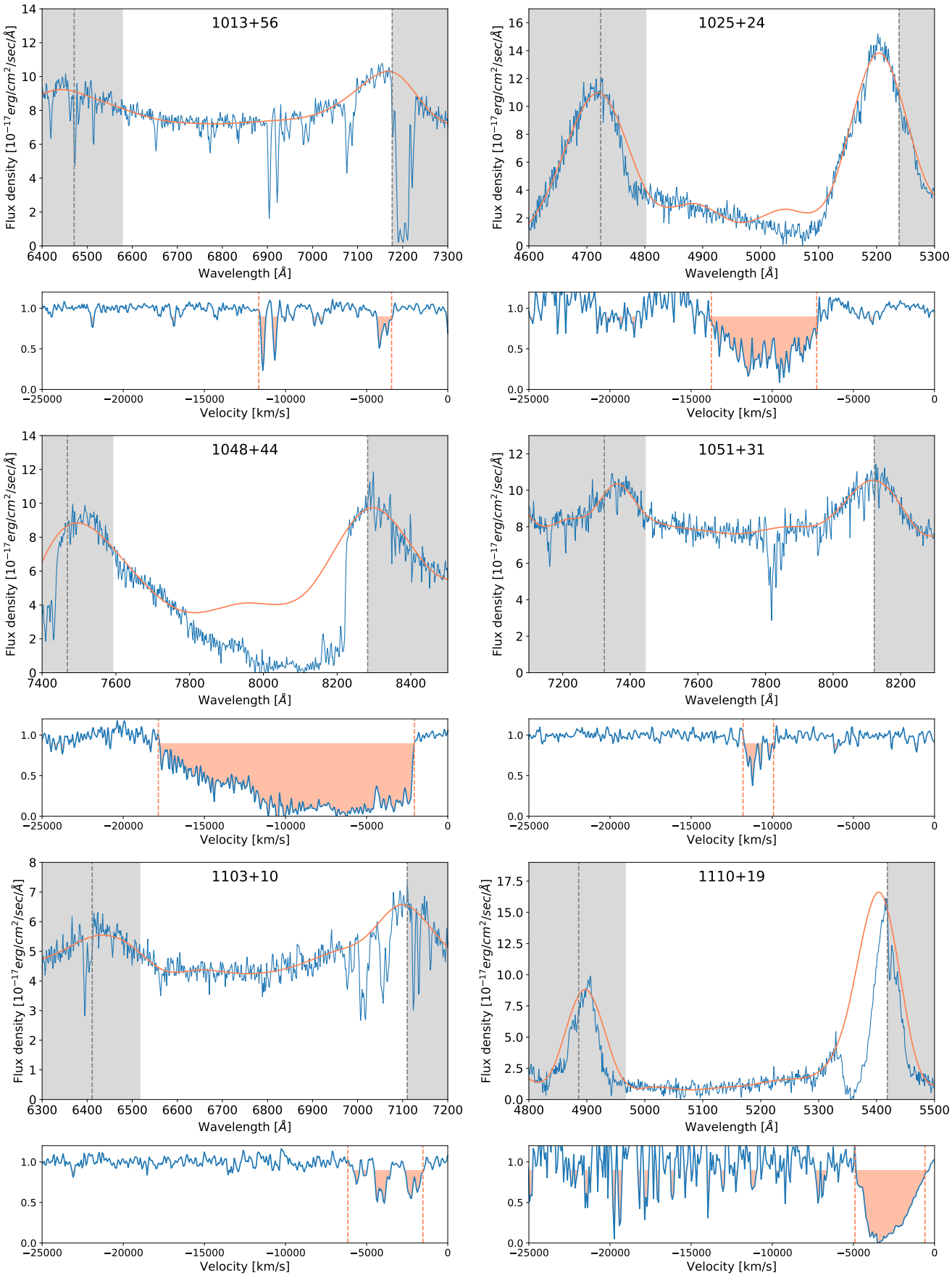

Fig. A.1. continued.

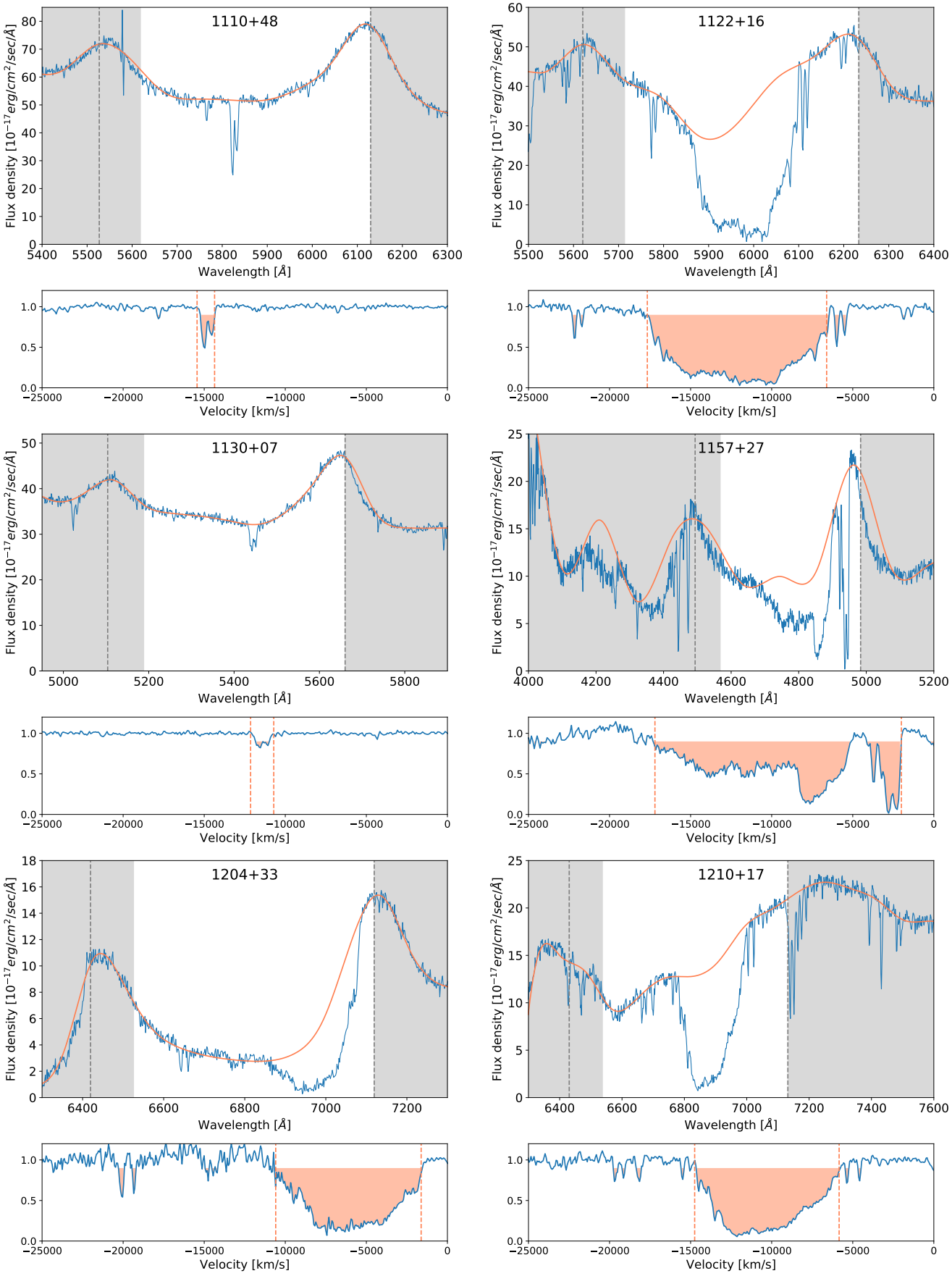

Fig. A.1. continued.

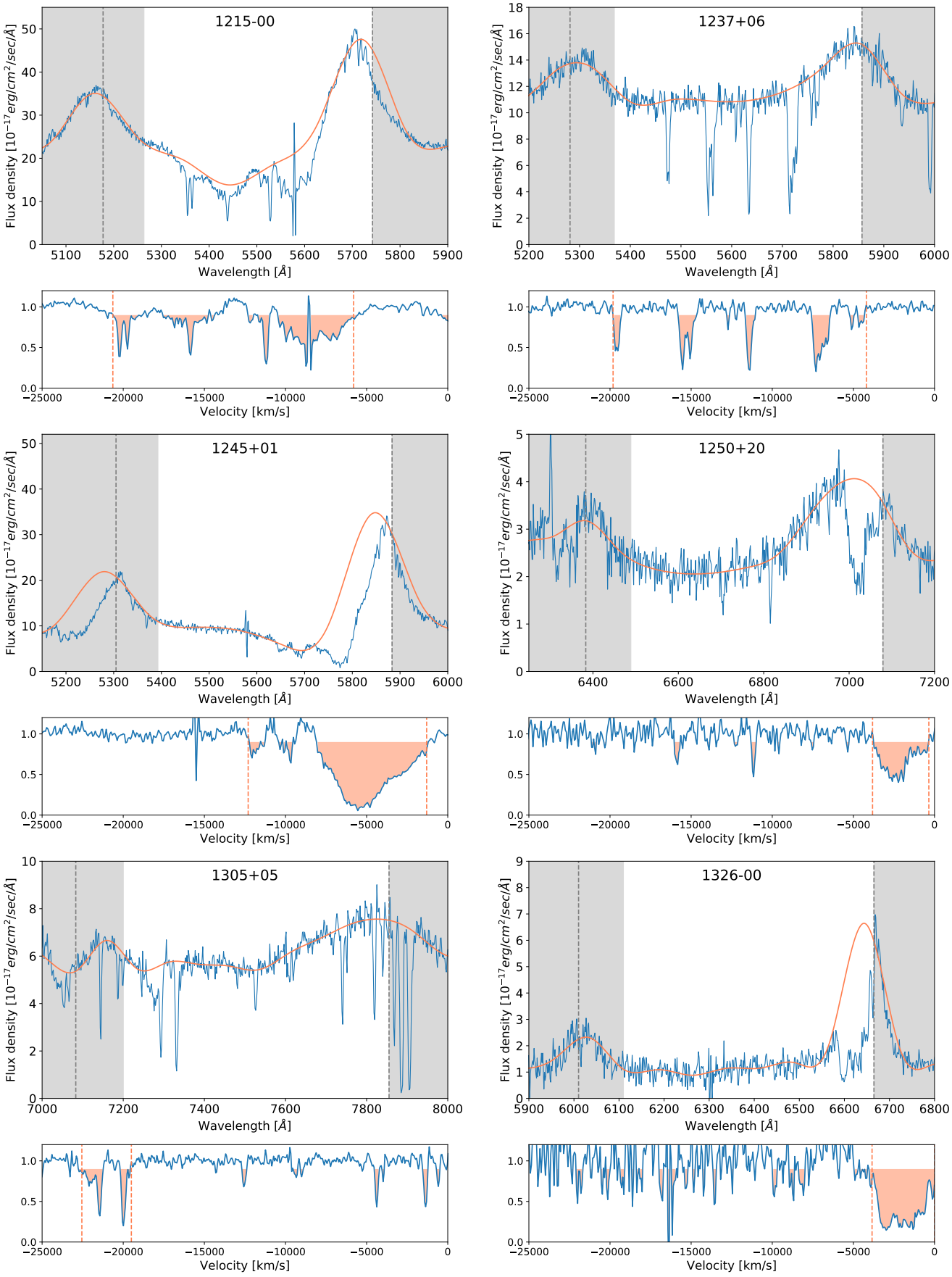

Fig. A.1. continued.

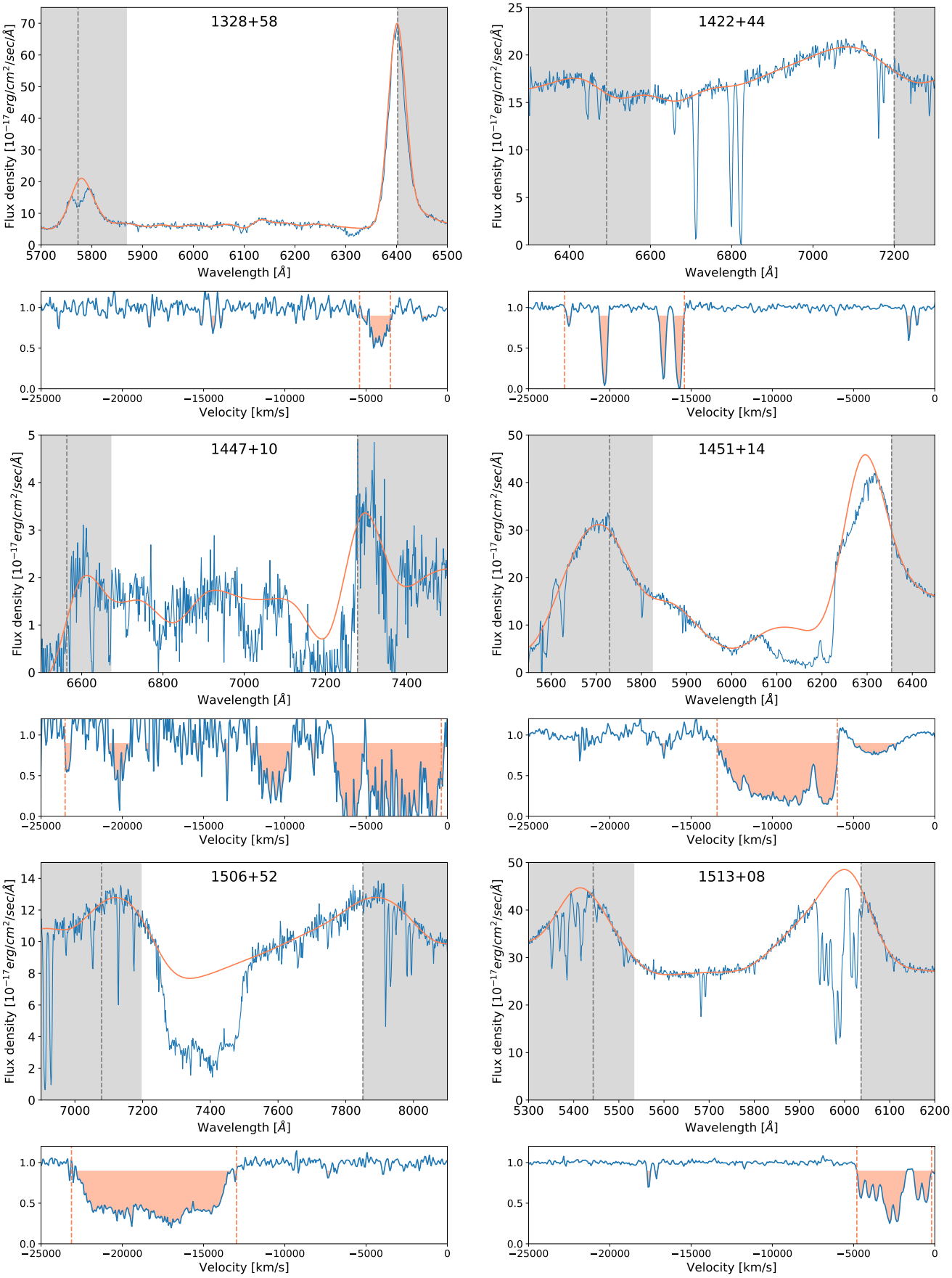

Fig. A.1. continued.

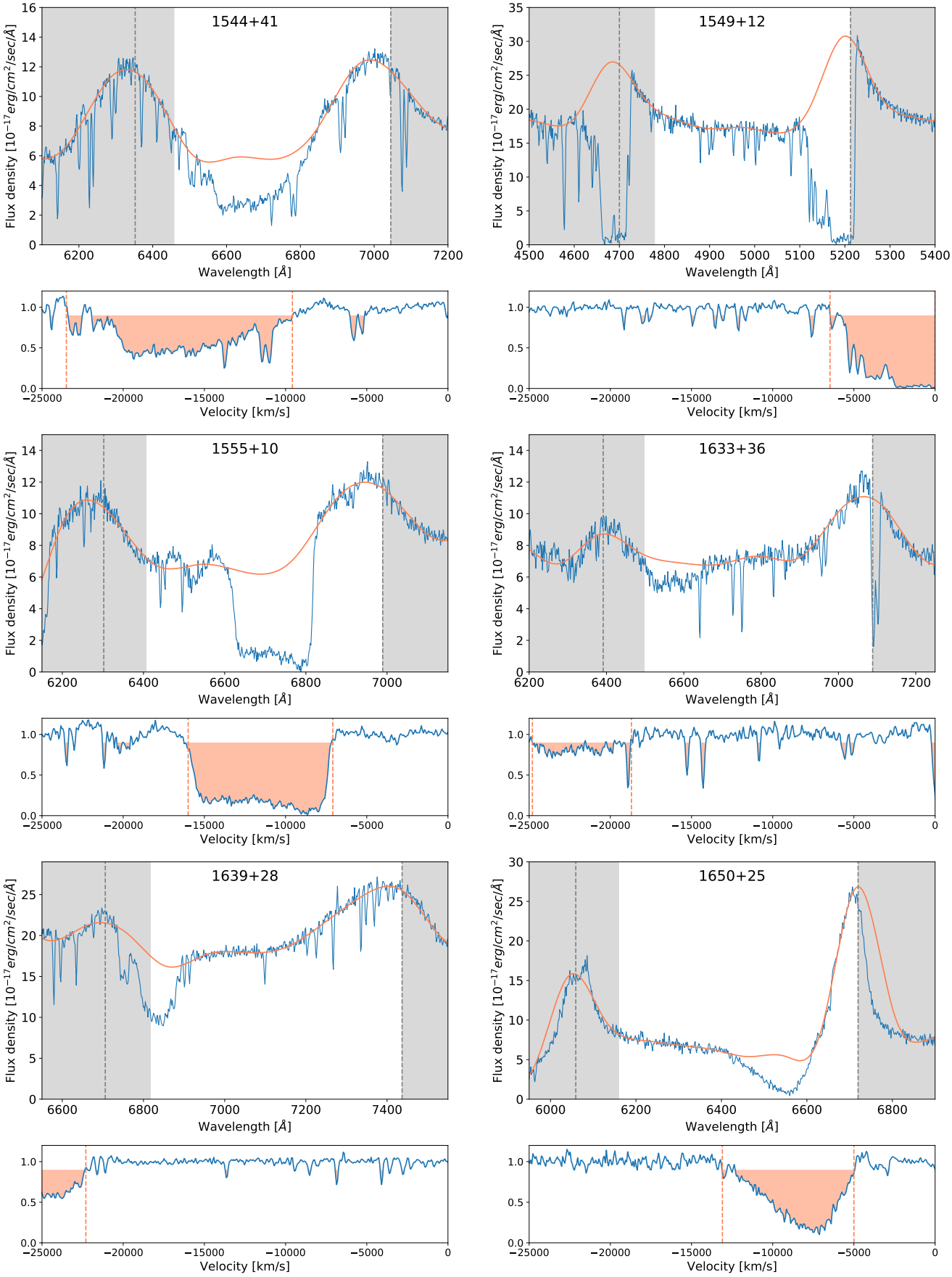

Fig. A.1. continued.

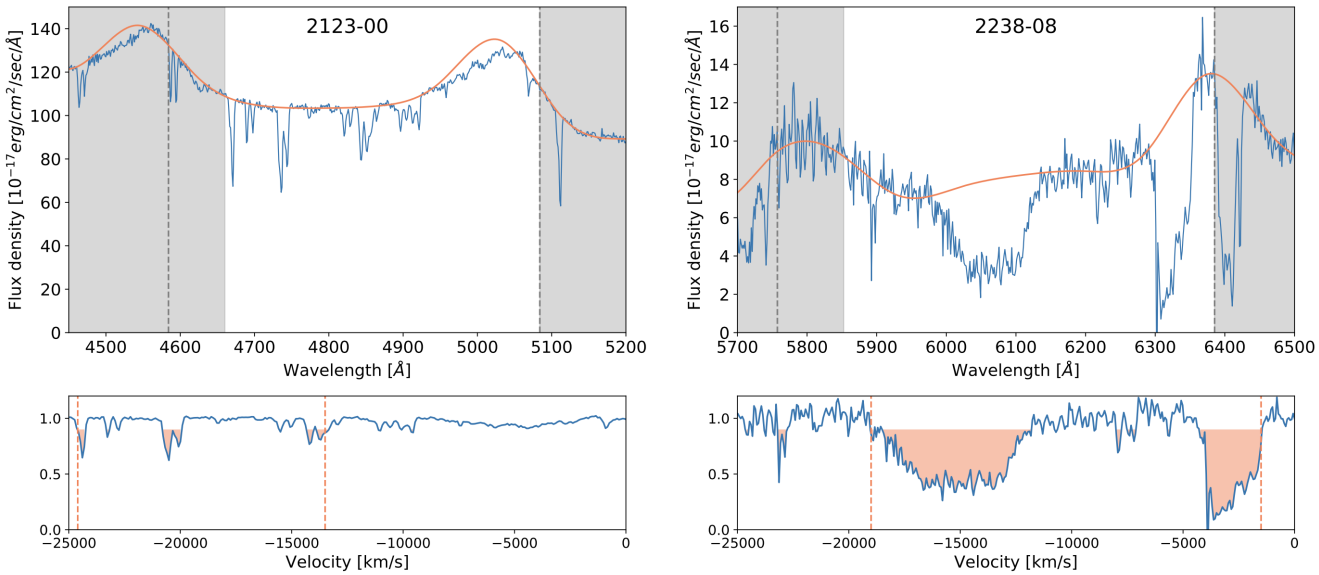

Fig. A.1. continued.